Title

Amyloid β-Protein Monomer Folding: Free-Energy Surfaces Reveal Alloform-Specific Differences

Journal

Journal of Molecular Biology, 384(2)

ISSN

0022-2836

Authors

Yang, Mingfeng
Teplow, David B

Publication Date

2008-12-01

DOI

10.1016/j.jmb.2008.09.039

Peer reviewed

doi:10.1016/j.jmb.2008.09.039 J. Mol. Biol. (2008) 384, 450–464

JMB

Available online at www.sciencedirect.com

ScienceDirect

ELSEVIER

Amyloid β-Protein Monomer Folding: Free-Energy Surfaces Reveal Alloform-Specific Differences

Mingfeng Yang and David B. Teplow*

Department of Neurology, David Geffen School of Medicine, and Molecular Biology Institute and Brain Research Institute, University of California, Los Angeles, Los Angeles, CA 90095, USA

Received 17 July 2008; received in revised form 9 September 2008; accepted 12 September 2008
Available online
24 September 2008

Alloform-specific differences in structural dynamics between amyloid β-protein (Aβ) 40 and Aβ42 appear to underlie the pathogenesis of Alzheimer's disease. To elucidate these differences, we performed microsecond timescale replica-exchange molecular dynamics simulations to sample the conformational space of the Aβ monomer and constructed its free-energy surface. We find that neither peptide monomer is unstructured, but rather that each may be described as a unique statistical coil in which five relatively independent folding units exist, comprising residues 1–5, 10–13, 17–22, 28–37, and 39–42, which are connected by four turn structures. The free-energy surfaces of both peptides are characterized by two large basins, comprising conformers with either substantial α-helix or β-sheet content. Conformational transitions within and between these basins are rapid. The two additional hydrophobic residues at the Aβ42 C-terminus, Ile41 and Ala42, significantly increase contacts within the C-terminus, and between the C-terminus and the central hydrophobic cluster (Leu17-Ala21). As a result, the β-structure of Aβ42 is more stable than that of Aβ40, and the conformational equilibrium in Aβ42 shifts towards β-structure. These results suggest that drugs stabilizing α-helical Aβ conformers (or destabilizing the β-sheet state) would block formation of neurotoxic oligomers. The atomic-resolution conformer structures determined in our simulations may serve as useful targets for this purpose. The conformers also provide starting points for simulations of Aβ oligomerization—a process postulated to be the key pathogenetic event in Alzheimer's disease.

Keywords: Alzheimer's disease; amyloid β-protein; protein folding; molecular dynamics; free-energy surface

Edited by D. Case

Introduction

Alzheimer's disease (AD) is the most common cause of late-life dementia.[1] The pathognomonic neuropathologic features of AD are extracellular amyloid deposits comprising primarily fibrils of the amyloid β-protein (Aβ) and intracellular neurofibrillary tangles formed by tau protein.[2] Compelling evidence supports a seminal role of Aβ in AD. Fibrils originally were thought to be central to AD pathogenesis,[3] but recent studies support the hypothesis that the proximate neurotoxic agents in AD are Aβ oligomers.[4–6] In fact, recent experiments have shown that some pathways of Aβ oligomerization and fibril formation are independent[7,8] and that fibrillization may be protective.[9]

Aβ is produced naturally and ubiquitously *in vivo* as an ~4-kDa peptide.[10] It exists predominately in two forms, Aβ40 and Aβ42, which contain 40 and 42 amino acids, respectively (Fig. 1). Despite the small structural difference between Aβ40 and Aβ42 (the C-terminal Ile-Ala sequence), the peptides display significantly different behaviors *in vitro* and *in vivo*. Aβ42 is the principal component in parenchymal plaques.[11–13] An increase in the Aβ42/Aβ40 concentration ratio is associated with familial forms of early-onset AD.[14,15] Treatments that reduce Aβ42 levels have been shown to correlate with a decreased risk for AD.[16] In addition, Aβ42 displays enhanced neurotoxicity relative to Aβ40.[17–19] *In vitro* studies have shown that Aβ42 displays fibril nucleation and elongation rates that are significantly higher than

*Corresponding author. E-mail address: dteplow@ucla.edu.

Abbreviations used: Aβ, amyloid β-protein; AD, Alzheimer's disease; MD, molecular dynamics; REMD, replica-exchange molecular dynamics; CHC, central hydrophobic cluster; GB, generalized Born.

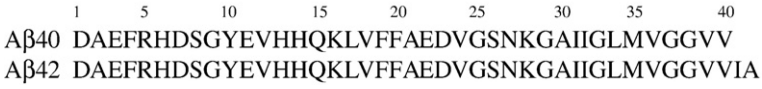

Fig. 1. The primary structures of Aβ40 and Aβ42. The sequences are displayed using a one-letter amino acid code, beginning from the left with the N-terminal Asp1.

those of Aβ40,[20–22] and that Aβ42 forms larger oligomers than does Aβ40.[23,24] These results support the conclusion that development of efficacious therapeutic agents for AD would be facilitated by knowledge in at least two areas: (1) the structural dynamics of Aβ monomer folding and oligomerization, and (2) differences in the dynamics between Aβ40 and Aβ42.

Experimental studies of Aβ monomer structure and dynamics are complicated by the lack of existence of a stable fold and the propensity of the peptide to aggregate into amorphous assemblies or multiple fibrillar forms.[25,26] NMR experiments on Aβ fragments or full-length Aβ40 and Aβ42 performed in the absence of solvent additives consistently reveal little regular structure.[27–35] A small increase in C-terminal rigidity has been observed in Aβ42 *versus* Aβ40.[34] Consistent with these data, studies of region-specific endoprotease sensitivity showed increased resistance of the Aβ42 C-terminus.[29] These studies have provided relatively coarse insights into local Aβ structure, but they were not capable of elucidating the Aβ conformational ensemble in atomic detail. Substantial helical structure was revealed in Aβ studied in mixtures of fluorinated alcohols[36–40] or SDS[41,42] with water. However, the relevance of these systems to understanding extramembranous assembly is unclear.

Molecular dynamics (MD) simulations complement experimental studies through their ability to define the conformational space and dynamics of a macromolecule(s).[43] This approach is being applied actively in the Aβ field (for recent reviews, see Teplow *et al.*[44] and Urbanc *et al.*[45]). Recently, we studied Aβ42 dynamics computationally, integrating these data with experimental results obtained using ion mobility spectroscopy–mass spectrometry.[46] We found that Aβ42 conformational space is dominated by loops and turns. Comparative studies with Aβ40 were not performed. Sgourakis *et al.* performed Aβ simulations using both Aβ40 and Aβ42 in an explicit water environment.[47] Structured regions were observed, one of which was a β-hairpin within the C-terminal peptide segment Ile31-Ala42. The simulation employed a virtual cubic space that was designed to contain a collapsed peptide that then was solvated by explicit water molecules. This system size may not accommodate extended conformers and thus not completely sample conformational space—a result that would produce a biased view of Aβ structure and dynamics. Here, using replica-exchange molecular dynamics (REMD) with an all-atom protein model, we sample and compare the conformational spaces and the corresponding free-energy surfaces of Aβ40 and Aβ42. We assess the relevance of the data by comparison with experimental information extant. Through comparison of the structural dynamics of Aβ40 and Aβ42, we establish their shared and distinct features. Finally, we discuss the implications of these findings for understanding and potentially controlling neurotoxic Aβ assembly.

Results and Discussion

Agreement between simulation and experiment

Before performing extensive analyses of our simulation data, we sought to establish their physical relevance by comparison with experimental data produced using NMR—the experimental method that has provided the highest-resolution structural information on Aβ. To do so, we used chemical shift values predicted from our simulations (δ_{sim}) and determined experimentally (δ_{exp}). The δ_{sim} values were predicted with the SHIFTS program,[48] based on the conformational ensemble collected at 278 K. We used δ_{exp} values of monomeric Aβ that had been measured at the same temperature and pH.[32] As shown in Fig. 2, the small standard deviations of the chemical shift values indicate the convergence of our simulation. The δ_{sim} values of the C^{α} and H^{α} atoms of both Aβ40 and Aβ42 were highly correlated with those observed experimentally. A strong correlation ($r = 0.942$) was also observed for the N^{α} atoms of Aβ40. The N^{α} chemical shifts of Aβ42 were less correlated ($r = 0.883$) than those of Aβ40, but remained well correlated with δ_{exp}. It is possible that the modestly weaker correlations of N^{α} atoms are illusory because the SHIFTS program is known not to consider all the factors contributing to N chemical shifts in proteins.[49] It is also possible that the decreased correlation of the Aβ42 δ_{sim} (N^{α}) data results from intermolecular interactions among monomers in aqueous solution in the NMR experiment (Dr. Michael Zagorski, personal communication). In conclusion, the high correlations observed between our *in silico* data and those produced experimentally indicate that our simulations reproduce the Aβ structural ensemble well.

Secondary structure of Aβ

We first calculated and compared the secondary structures of Aβ40 and Aβ42. The secondary structure was assigned according to criteria defined by STRIDE[50] (Fig. 3) or DSSP[51] (Fig. S1). Both programs yielded qualitatively similar secondary structure assignments (see below). STRIDE defines a higher percentage of "turn" structure. This is

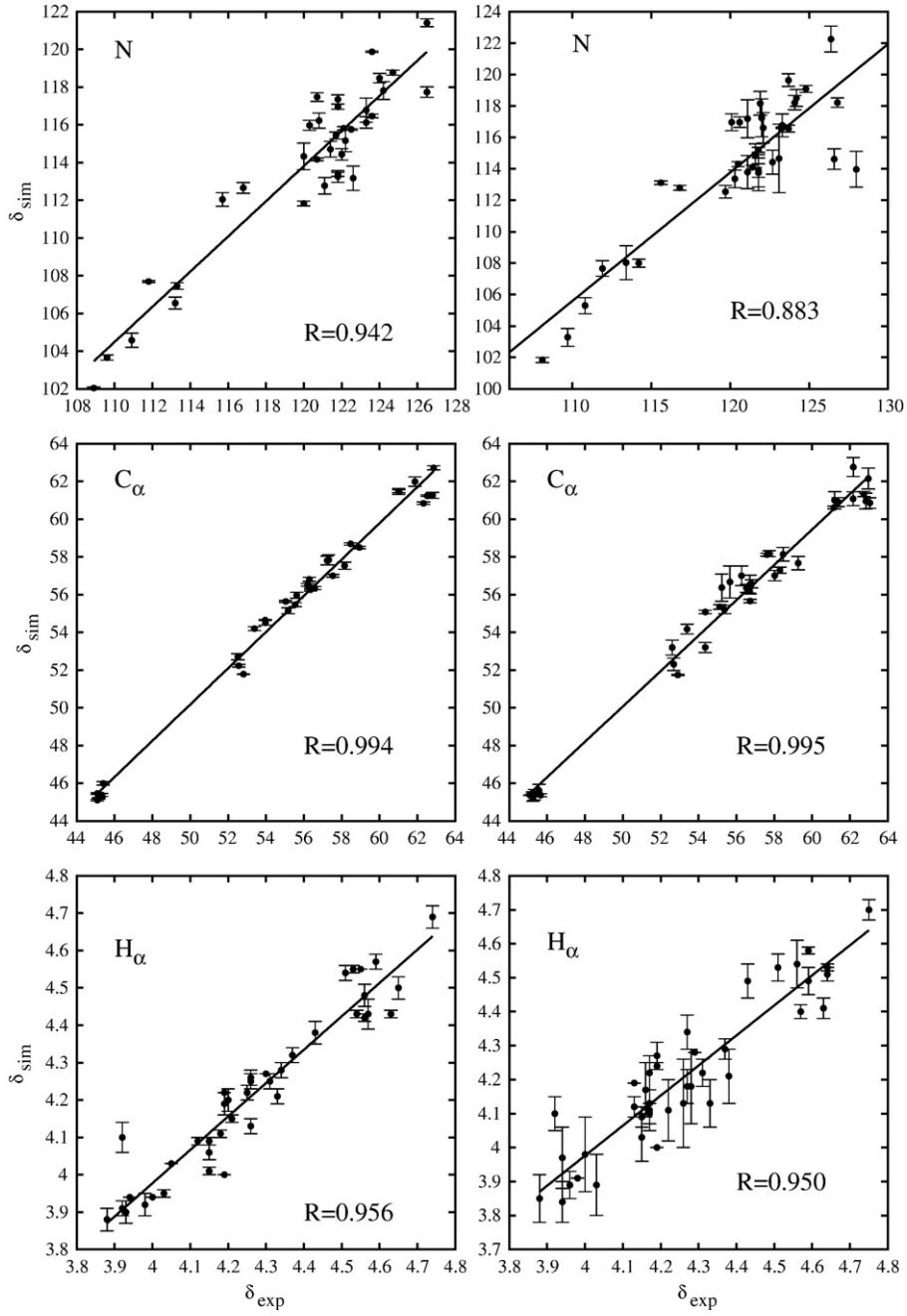

Fig. 2. Correlation of simulated and experimental chemical shifts. Chemical shift values were determined using the SHIFTS program[48] following REMD (δ_{sim}) and were compared with values measured experimentally at 278 K by NMR (δ_{exp}).[32] The Pearson correlation coefficient (r) is listed at the bottom right of each panel. Left: Aβ40; right: Aβ42. We divide the 100-ns trajectory into three 33-ns frames and calculate the standard deviations of the chemical shifts from the three samples. Small standard deviations indicate the convergence of our simulation.

consistent with the fact that distance criteria are used by STRIDE to assign turn structure, whereas DSSP uses H-bonding as a criterion. Turns defined by DSSP thus comprise a subset of all turns defined by STRIDE. Because Aβ is very dynamic conformationally, it does not display high levels of classical α-helix, β-strand, or β-turn. Therefore, to represent both classical and nonclassical turn structures, we discuss here the results obtained using STRIDE. The term "turn" thus refers to short peptide segments in which the peptide chain reverses direction, regardless of the presence or the absence of H-bonds.

Residues 6–40, except those at the N- or C-termini, exist as turn structures with ~30–80% probability. Residues more likely to exist as β-strand or α-helix are those at or adjacent to the central hydrophobic cluster (CHC) region (residues 17–21) and C-terminus (residues 30–36). In the CHC, a significant (≈30–40%) secondary structure comprising these types was observed. Residues 16–27 and 30–36 of Aβ42 display β-structures with frequencies of

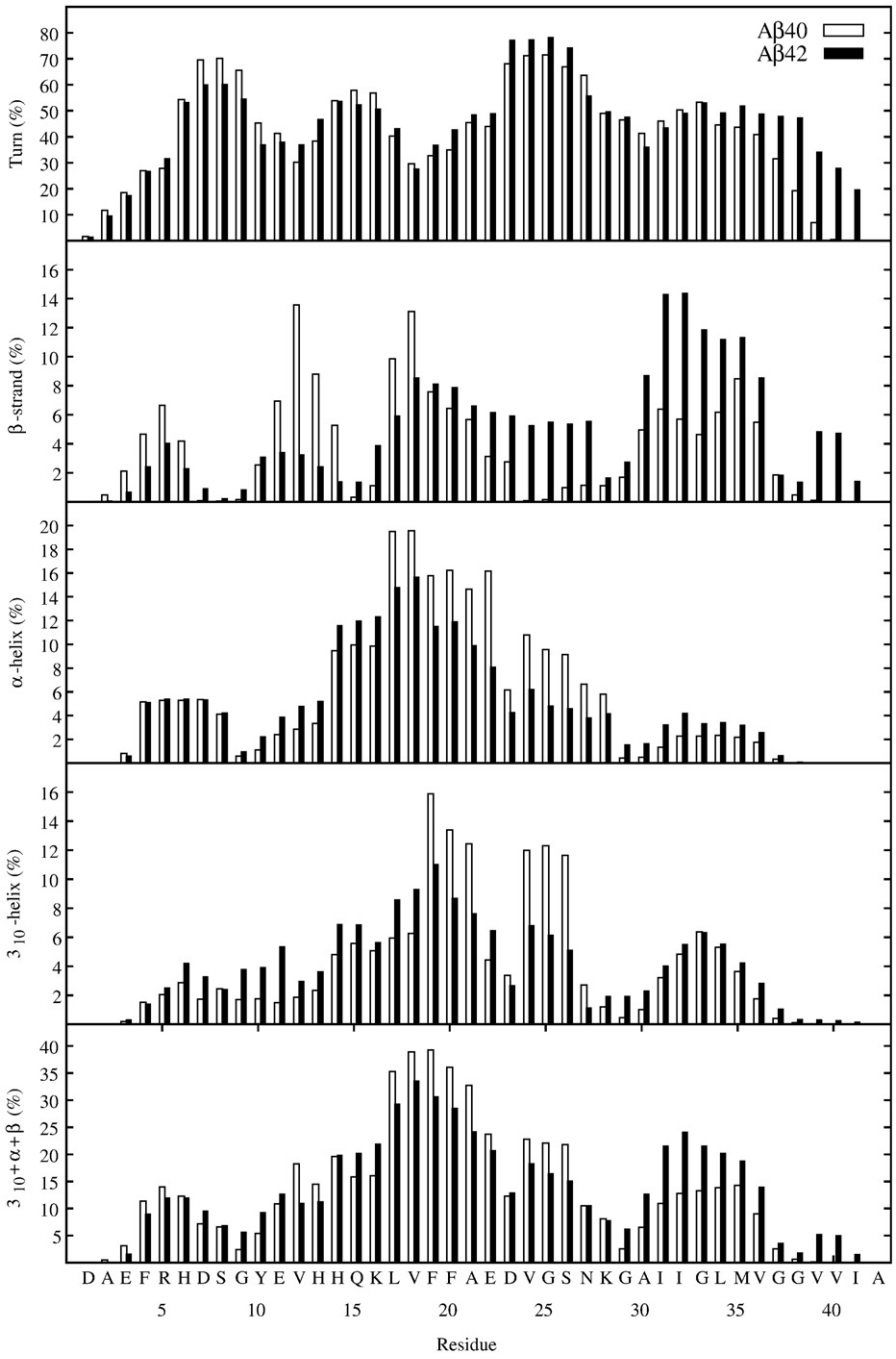

Fig. 3. Secondary structure of Aβ. Secondary structure occurrence frequencies for Aβ40 (white) and Aβ42 (black) were determined using the STRIDE program[50] following REMD simulation. Turn, β-strand, α-helix, 3_{10}-helix, and total secondary structure (3_{10}-helix + α-helix + β-strand) are shown. The frequencies of other structures were negligible (<0.1%).

~6–8% and ~8–14%, respectively. These data are consistent with prior experimental studies that have suggested that Aβ belongs to the class of "natively disordered" proteins.[52] However, Aβ is not entirely a "random coil." Two highly populated (>60%) turn structures, centered at residues 6–9 and 23–27, were observed. The positions of these turns correspond precisely with turn or bend-like structures observed by NMR to occur at Asp7-Glu11 and Phe20-Ser26.[32] We found that residues 14–16 and 31–35 also had high probabilities of existing as turns.

One experimental approach that has been used successfully to identify structured and unstructured regions within Aβ is limited proteolysis. This approach revealed a protease-resistant decapeptide segment, Ala21-Ala30, that was found in NMR studies to form a turn-like structure.[29] This region was postulated to nucleate folding of the Aβ monomer. Interestingly and consistent with this interpretation, pathogenic (linked to familial AD or cerebral amyloid angiopathy) amino acid substitutions within this region alter the stability of this

turn.[53] Based on these experimental findings, simulations of turn dynamics have been performed on the decapeptide.[54–56] These studies all revealed that a majority of the peptide conformers possess a turn-like structure that is stabilized by hydrophobic interactions between Val24 and Lys28 and by electrostatic interactions between Glu22 or Asp23 and Lys28. Baumketner *et al*. have suggested that hydrogen bonds involving the side chain of Asp23 and the amide hydrogen atoms of adjacent residues are important in stabilizing this turn.[46] These hydrogen bond interactions also recently were reported by Fawzi *et al.*, although their data suggested a lower occurrence frequency (~40%) for this type of conformer.[57] A stable turn formed by residues Val24-Asn27 and an intramolecular Asp23-Lys28 salt bridge also were observed in computational studies of Aβ(10–35) structural dynamics.[58]

Experiments on the Ala21-Ala30 decapeptide or on Aβ(10–35) cannot reveal effects of adjacent (missing) regions of the peptide that may occur in the biologically and clinically relevant full-length peptide. To determine whether such effects exist, we studied the structure and dynamics of the decapeptide turn element within the native Aβ monomer (Fig. 4). We found that the structure of residues 21–30 is highly similar (RMSD ≈ 1.0 Å) to that obtained using the decapeptide alone.[55] The structure is stabilized by an H-bond network involving the side-chain carboxyl oxygen atoms of Asp23 and the $N^{\alpha}H$ atoms of the adjacent residues Gly25, Ser26, Asn27, and Lys28 (Table 1); an H-bond between the Asp23 O^{γ} and the Ser26 H^{γ} atoms; and a salt bridge formed between the Lys28 N^{ζ} and the Glu22 carboxylate anion. Similar structural features and stabilizing factors also were observed in simulations by two other groups in explicit

Table 1. Asp23 hydrogen bond frequencies

Hydrogen bond pair	Aβ40 (%)	Aβ42 (%)
Asp23 O_{γ}···HN Val24	20.0	18.6
Asp23 O_{γ}···HN Gly25	27.4	35.9
Asp23 O_{γ}···HO_{γ} Ser26	75.2	70.3
Asp23 O_{γ}···HN Ser26	38.2	46.3
Asp23 O_{γ}···HN Asn27	18.5	20.9
Asp23 O_{γ}···HN Lys28	16.5	17.8
Asp23 O_{γ}···HN Gly29	12.3	13.5

The occurrence frequencies are listed for hydrogen bonds in the network involving the Asp23 O_{γ} atom.

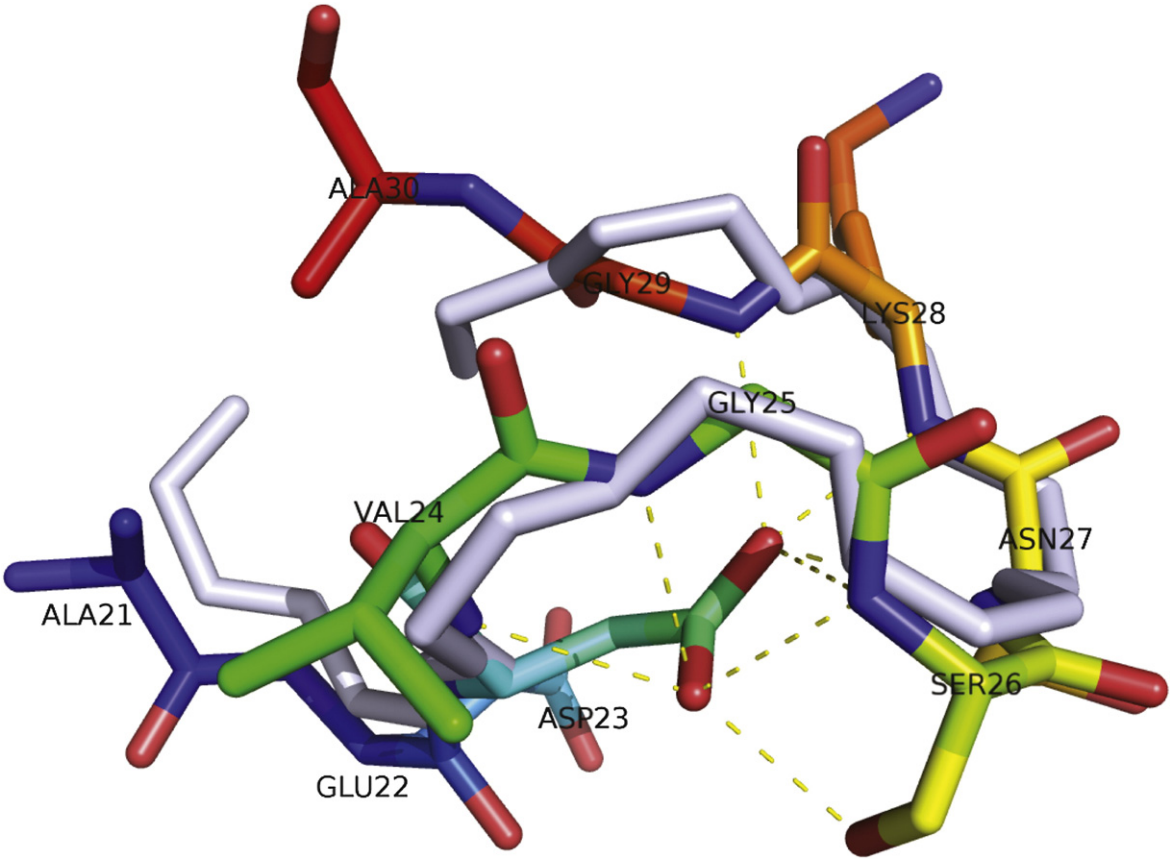

Fig. 4. A typical central turn structure formed by residues 21–30. Dashed yellow lines indicate hydrogen bonds stabilizing the turn structure. The frequency of each hydrogen bond is shown in Table 1. The turn structure, occurring with a probability of ≈28% in full-length Aβ40 and ≈23% in full-length Aβ42, is similar (RMSD ≈ 1. 0 Å) to that found in the most populated conformational cluster (gray) populated by the Aβ(21–30) decapeptide in simulations by Baumketner *et al.*[55]

solvent, one using the OPLS-AA force field[47] and the other using the Gromos force field (Dr. Yundong Wu, personal communication).

Our simulations suggest that Aβ(21–30) adopts similar structures in its isolated decapeptide form and in the context of the full-length Aβ monomer. In practice, this result suggests that the decapeptide is a relevant proxy for the cognate segment within the Aβ monomer. In theory, our observation would be predicted for a structural domain that serves to nucleate protein folding. It *should* fold in isolation, and this folding should not be affected significantly by adjacent regions. In the full-length peptide, decapeptide folding would facilitate contacts between the CHC and the C-terminal regions of Aβ—contacts that comprise key stabilizing elements of fibril structure. However, this fold forms infrequently, as Aβ exists in many conformations with comparable free energies and does not display a dominant global minimum on its free-energy surface (Fig. 8).

In our simulation, the C-terminus of Aβ42 is significantly more structured than that of Aβ40, as reflected by a higher percentage of turn structure within peptide segment 34–41 and of β-structure within segment 30–42. It is noteworthy that residues 30–36 in Aβ42 have almost twice the β-structure that they do in Aβ40 and that residues 39 and 40 have no β-structure in Aβ40, whereas they can exist in β-structure in Aβ42 with a likelihood of ~5%. The more frequent turn and β-structure at the Aβ42 C-terminus may be due to increased intramolecular contacts stabilized by the two hydrophobic residues Ile41 and Ala42. In fact, such stabilizing interactions may account for the increased C-terminal rigidity observed in NMR experiments.[32–34] Higher β-structure frequency is observed also among residues 20–27 of Aβ42, the basis of which is a β-hairpin centered at residues 28 and 29 (Fig. 8b, cluster 8). Cluster 8 does not exist with Aβ40. Interestingly, residues 3–6, 11–14, and 17–18 have higher β-content in Aβ40 than in Aβ42, and residues 17–28 are more likely to exist in α-helices in Aβ40. For both peptides, residues 14–28 are more likely to form an α-helical structure than the C-terminus, consistent with a number of experiments in which central region α-helices were more stable than C-terminal helices.[40]

Tertiary structure

We assess tertiary structure by analyzing contacts among amino acids (Fig. 5). Two amino acids were considered in contact if any heavy atom (C, N, O, or S) of one residue was ≤5 Å from any heavy atom of the other residue. Globally, the contact maps of Aβ40 and Aβ42 are similar and are characterized by relatively frequent contacts of residues *within* peptide segments 3–13, 10–20, and 17–36 (Fig. 5, red boxes). These segments correspond to populated turn structures centered at residues 6–9 (T_1), 14–16 (T_2), and 23–27 (T_3), respectively. Weaker but noticeable contacts also were observed *between* two discontinuous segments, 6–10 and 23–27. We note that the CHC contacts residues 30–36 at the C-terminus with 20–30% probability. However, with the two extra residues Ile41-Ala42 at the C-terminus, residues 30–42 of Aβ42 are more likely to contact each other, presumably in the context of a turn (Fig. 5b).

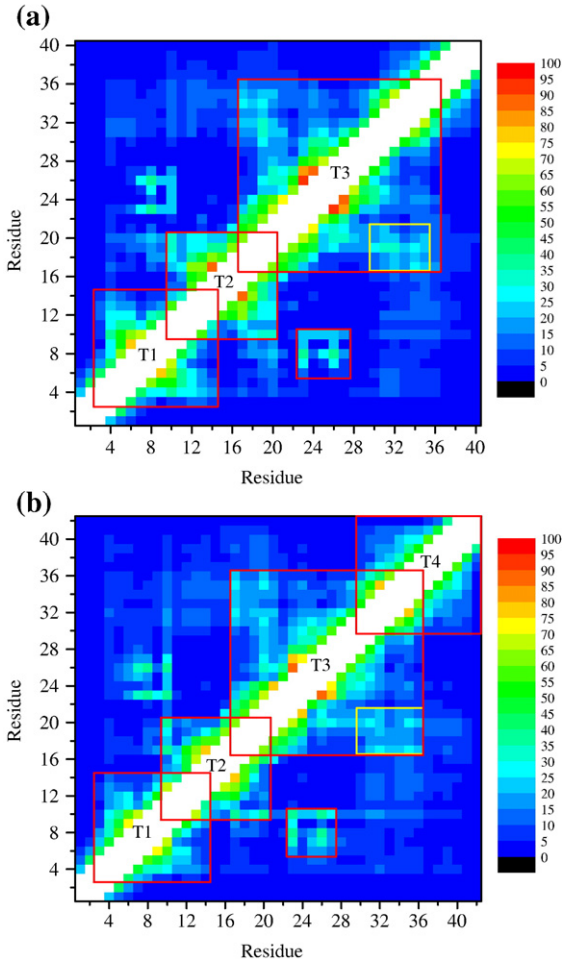

Fig. 5. Intramolecular contact maps. Bimolecular contact frequencies between amino acids in monomers are shown for (a) Aβ40 and (b) Aβ42. The contact frequency is color-coded (scale to the right of each panel) with a spectral range from black (0%) to red (100%). Red squares in each panel demarcate the peptide segments 3–13, 10–20, and 17–36 corresponding to three populated turn regions T_1, T_2, and T_3 in which frequent contacts are observed. Contacts within the C-terminus of Aβ42 (residues 30–42) also are frequent as a result of turn formation (T_4). The boxes located on the abscissa at 23–27 (red) and centered at ≈33 (yellow) highlight significant but weaker interseg-ment interactions (see the text).

Despite the overall global similarity in contacts between Aβ40 and Aβ42, differences are discernible (Fig. 6, red boxes). Residues 24–30 of Aβ40 are more compact than those of Aβ42, as shown by 2.5–30% more contacts in this region (Fig. 6a). This is consistent with the higher helical content of this region (Fig. 3). The Aβ40 CHC is more likely (5–17.5%) to contact the N-terminus. In contrast, the Aβ42 CHC is 2.5–10%

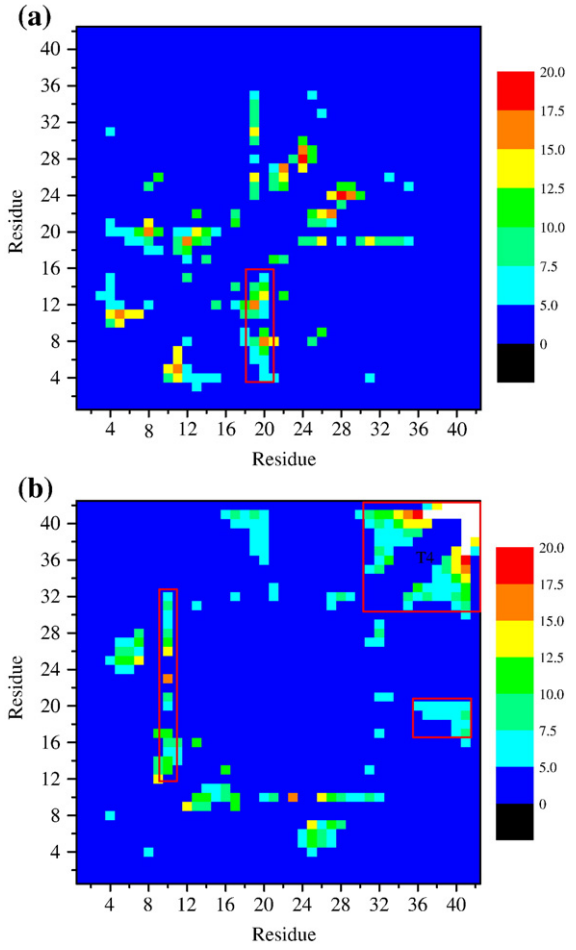

Fig. 6. Difference maps. Simple arithmetic subtraction of the intramolecular contact frequencies in Aβ42 from those in Aβ40, or vice versa, reveals residue pairs with greater contact frequencies in (a) Aβ40 or (b) Aβ42, respectively. Frequencies (%) are color-coded according to the scales shown. Red boxes highlight alloform-specific contacts.

more likely to contact the C-terminus (residues 34–41) (Fig. 6b). Residues 3–8 contact residues 10–14 more frequently, corresponding to higher turn formation of residues 6–9 and higher β-content of residues 2–14. A peculiar residue is Phe19, which is more buried in Aβ40, as evidenced by its more frequent contacts with residues 3–36.

The extra two residues at the C-terminus significantly increase the contact frequency within peptide segment 31–42 and also increase modestly the contact frequency between the C-terminus and the CHC. It is interesting to note that Tyr10 in Aβ42 contacts residues 13–32 more frequently (Fig. 6b, red box), suggesting that it is more shielded from the solvent. In fact, recent chemical cross-linking experiments suggest that Tyr10 is more difficult to cross-link in Aβ42 than it is in Aβ40 (unpublished observation).

Contact maps (Fig. 5) suggest that the N-terminus of Aβ40 is more compact than that of Aβ42, whereas the opposite is true of the C-terminus. MD simulations of Aβ oligomerization performed by Urbanc *et al.* showed that the N-termini of Aβ42 monomers comprising oligomers were significantly more extended and unstructured than those in the corresponding Aβ40 assemblies.[59] Our observation here suggests that this feature exists at the monomer level. We postulate that the increased hydrophobicity of the Aβ42 C-terminus, due to the presence of Ile41 and Ala42, increases the contact frequency between residues in the C-terminus and the CHC. As a result, the N-terminus of Aβ42 has less contact with the CHC and exists most frequently as an extended or coil structure. This postulation is consistent with results of studies of the assembly state dependence of the intrinsic fluorescence of a Tyr residue substituted for Phe20.[60] These studies showed that a significant increase in fluorescence intensity occurred in Aβ40, but not in Aβ42, during the initial oligomerization of the peptides. This change would result from a disruption of the N-terminus–CHC interaction in the Aβ40 monomer and the subsequent formation of the more apolar CHC–C-terminus complex, in which quenching of the fluorescence would be substantially lower. It is intriguing that recent scanning cross-linking studies have suggested that such competition between the N-terminus and the C-terminus for interaction with the CHC is a fundamental feature of Aβ conformational dynamics.[61] In Aβ42, relative to Aβ40, the C-terminus "wins" because the presence of Ile41 and Ala42 facilitates formation of a C-terminal bend that creates a larger and more stable hydrophobic region—one that can interact especially strongly with the CHC. The biological consequence of this interaction is the formation of folded Aβ monomers with the well-known increased propensity to form neurotoxic higher-order assemblies.

Correlated motion

Secondary and tertiary structure analyses suggest that Aβ is relatively disordered and thus populates a large conformational space. However, like proteins in general,[62,63] and from the computational and experimental results discussed above, the Aβ monomer does not appear to be a random coil, if we define "random coil" as an entity that can populate every point in monomer conformational space with equal probability. The implication of this fact is that valuable knowledge may be obtained if nonrandom features of conformational space can be identified. One method to achieve this goal is to identify segments of Aβ whose motions are correlated. To do so, we quantify the cross-correlations of atomic positional fluctuations.[64] This approach has shown that many regions in proteins, especially those involving secondary structure elements, display correlated motions.

We represent each residue with its corresponding C^{α} atom. In Fig. 7, each grid square indicates the correlation ($\mathbf{r}_{ij}$) between a residue pair. $\mathbf{r}_{ij}=1$ indicates

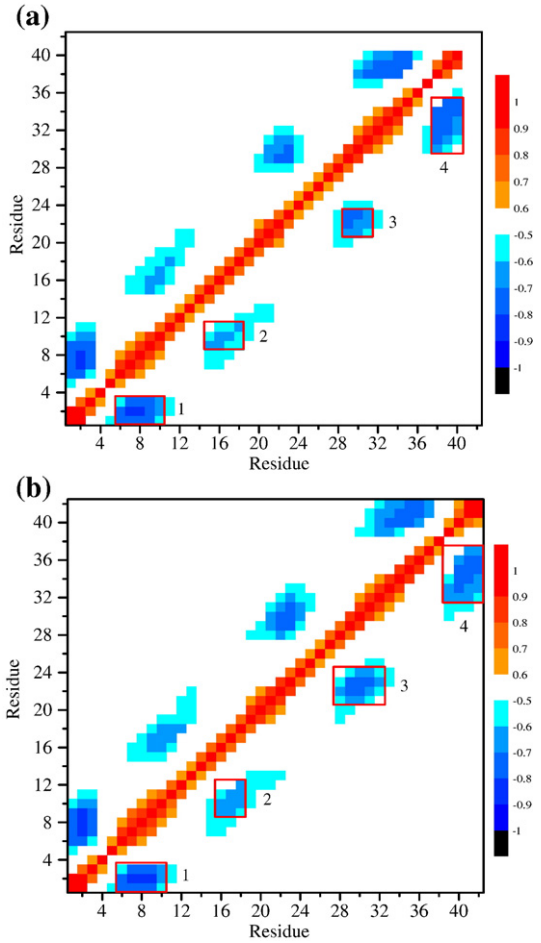

Fig. 7. Cross-correlation of atomic positional fluctuations. Intramolecular cross-correlation coefficients are shown for (a) Aβ40 and (b) Aβ42. The motion of a residue pair is considered correlated if its corresponding correlation coefficient ($\mathbf{r}_{ij}$) has an absolute value of ≥ 0.5. Red boxes highlight strong anticorrelated motions.

that two residues are completely correlated, whereas $\mathbf{r}_{ij}=-1$ indicates completely anticorrelated motions. Complete correlation means that two residues always move together with the same phase and period. For simplicity, we arbitrarily define meaningful correlations to be those with $|\mathbf{r}_{ij}| \geq 0.5$.

For both Aβ40 and Aβ42, positive correlations are observed only along the diagonal line (i.e., residues have motions that are correlated only with their immediate neighbors). All nonneighbor motions are anticorrelated. Aβ40 and Aβ42 each display four sets of peptide segments whose motions are correlated significantly (Fig. 7, red boxes 1–4). The location of each set is similar, but the sizes of the sets and the magnitudes of the correlations within them vary (Fig. 7, Table 2). In Aβ40, the largest negative correlations exist between residues 1–3 and 6–10 (box 1; T_1), between residues 9–11 and 15–18 (box 2; T_2), between residues 21–23 and 29–31 (box 3; T_3), and between residues 30–35 and 38–40 (box 4; T_4). The correlations in boxes 1 and 2 of Aβ42 occur over a similar segment range as do those in Aβ40 and have similar total magnitudes. The largest difference occurs for box 3, in which substantially greater total correlation exists for Aβ42. The segment range in box 4 is translated two residues towards the C-terminus in Aβ42 relative to Aβ40, and the total correlation magnitude is greater. These differences result from the presence of Ile41 and Ala42, which likely stabilize a C-terminal turn centered at Gly38. This postulation is consistent with our secondary structure analyses (Fig. 3), which show that residues adjacent to the Gly37-Gly38 dipeptide in Aβ42 have particularly high probabilities of forming β-structures.

If monomer tertiary structure is maintained during peptide oligomerization and fibril formation, our data allow certain structure–activity predictions. For example, models of Aβ fibril structure produced using NMR data suggest that the fibril is formed by parallel in-register packing of β-strand–turn–β-strand motifs[65,66] in which D23-K28 salt bridges stabilize the turn. The formation of the T_3 turn identified in our simulation would increase contacts between peptide segments immediately adjacent to it, facilitating fibril formation. In contrast, formation of the T_4 turn (centered at Gly38) would disrupt the extended conformation that exists in the C-terminal β-strand element of the fibril. In considering these predictions, however, it is important that Aβ conformational dynamics in the monomer state be distinguished from that in the fibril state. The two are related, but the most stable conformers in one state are not entirely isomorphous with those in the other. Experimental and computational studies have shown that conformational conversions may occur both in incoming monomers attaching to fibril ends and in the monomers comprising the fibril ends themselves.[67–69]

Our observation that all the negatively correlated peptide segments reside on the opposite sides of turns identified at residues 6–9, 14–16, and 23–27 (Fig. 3) suggests that segmental motion within Aβ is dominated by "zipping" and "unzipping" motions around these turn structures. It is intriguing to consider Aβ monomer folding as a process involving five relatively independent folding units (residues 1–5, 10–13, 17–22, 28–37, and 39–42) that are connected by four turn structures. This simple consideration would have a highly significant

Table 2. Total cross-correlation magnitude

Box	Aβ40	Aβ42
1	−10.9	−11.0
2	−6.8	−7.2
3	−7.6	−12.2
4	−12.1	−14.7

To enable a quantitative comparison of segmental cross-correlations, boxes that delineated regions of the highest residue cross-correlations (Fig. 7, boxes 1–4) were created. The total cross-correlation magnitude within each box then was determined according to $\mathbf{r}_{\text{total}} = \sum_{k=1}^{n} \mathbf{r}_{ijk}$.

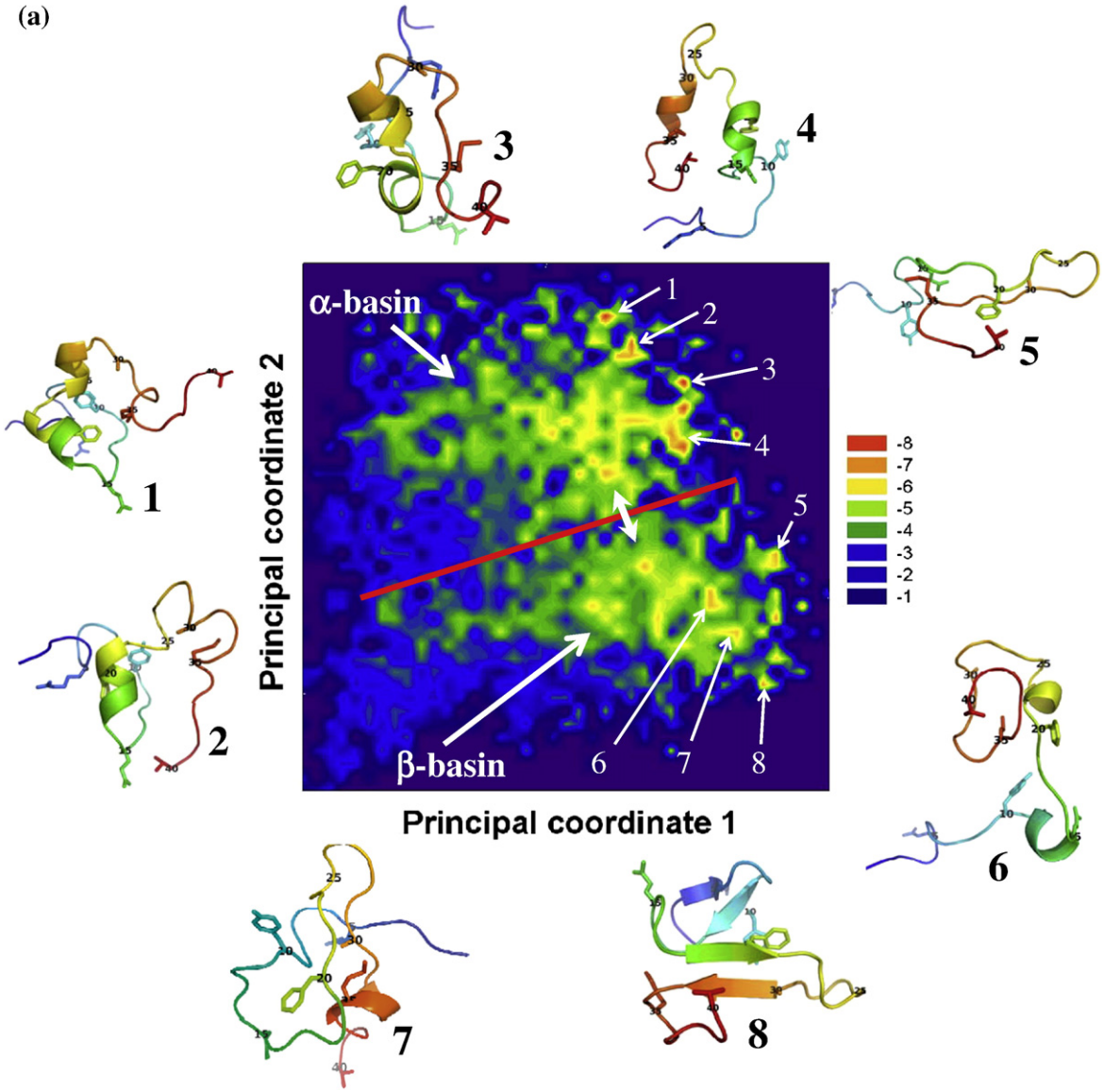

Fig. 8 *(legend on next page)*

implication: the degrees of freedom† for Aβ folding would decrease from ~2000 to ~10, and this would enable *ab initio* determination of the structures of higher-order assemblies such as Aβ oligomers, now thought to be the proximate neurotoxins in AD.[10]

Free-energy surface

To facilitate our understanding of the conformational equilibria of Aβ, we used principal coordinate analysis[70] to project its conformations onto a two-dimensional space comprising the first two principal coordinates. By defining a third coordinate as conformational free energy, we constructed the free-energy surface for Aβ (Fig. 8). This method has been shown to effectively preserve the essential features of the conformational space. Surfaces of Aβ40 and Aβ42 share two global features: (1) two large basins, one dominated by extended or β-sheet conformations ("β-basin") and the other dominated by α-helical structures ("α-basin;" except position 8 in Fig. 8b); and (2) a number (~20) of minima that have comparable free energies and are separated by shallow barriers. This latter feature predicts that conformational conversions (movement among these minima) occur frequently.

The first principal coordinate of Aβ40 dominates the conformational conversion within each basin, and the α-helix→β-sheet conversion occurs along the second principal coordinate (Fig. 8a, white double-headed arrow). In contrast, the α-helix→β-sheet conversion of Aβ42 occurs along its first

† We calculate degrees of freedom $df = 3N - 6$, where N is the number of elements in the system. For Aβ42, N = 630, where N is the number of atoms in the peptide. For a system with five folding units, $N = 5$ if the structures of the units are known.

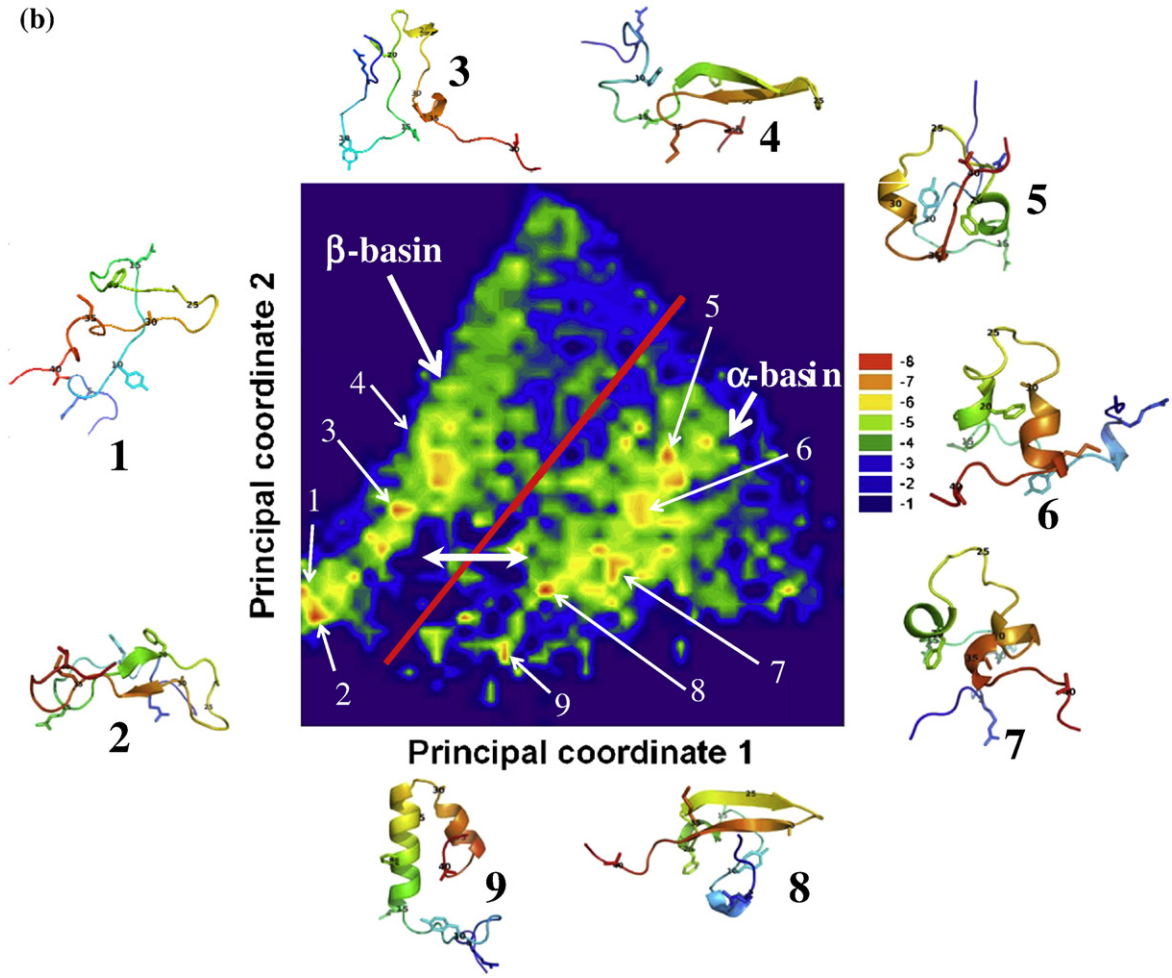

Fig. 8. Free-energy surfaces. (a) Aβ40; (b) Aβ42. Both surfaces exhibit two large basins: an α-basin and a β-basin. Red lines have been superimposed on the figures as gross indicators of the interfaces between the basins. White double-headed arrows denote the direction of the conformational transition between the two basins. Representative conformers from a number of low-energy wells are enumerated with black numbers outside of each panel, and the corresponding well within the panel itself is indicated by a white arrow and number. The positions of the amino acids in each conformer are indicated spectrally, from the N-terminus (indigo) to the C-terminus (red), and by small black residue numbers. Topological analyses of the Aβ40 and Aβ42 surfaces allow comparisons to be made of the distributions of conformers and their stabilities. The reader should note, however, that no formal correspondence exists between the principal coordinates in each system.

principal coordinate, and conformational conversions within the α- or β-basins occur along the second principal coordinate (Fig. 8b, white double-headed arrow). This suggests that α-helix→β-sheet transitions occur more readily in Aβ42 than in Aβ40.

We also see that the local minima in the Aβ40 α-basin have lower free energies, on average, than those in the β-basin (Fig. 8a), whereas for Aβ42, the magnitudes of the free energies of local minima in both basins, on average, are comparable (Fig. 8b). Previous experimental studies have shown that α-helix-containing conformers are obligatory but transitory intermediates in Aβ fibril assembly, both for Aβ40 and for Aβ42.[71] During fibril assembly, in which a statistical coil→α-helix→β-sheet conformational conversion path is observed, the maximum α-helix content of Aβ40 and Aβ42 was 32% and 19%, respectively, and Aβ42 reached its maximal α-helix content significantly sooner than did Aβ40.[71] Consistent with this finding, solvent conditions that facilitate the *initial* coil→α-helix transition significantly accelerate fibril assembly, whereas increased α-helix stabilization blocks β-sheet formation.[72] The thermodynamics of these systems revealed in the respective energy surfaces provides a mechanistic explanation for this observation. First, the deeper α-helix basin in Aβ40 means that Aβ40 conformers will populate these regions more frequently. Second, the lower barriers for α-helix→β-sheet transitions in the Aβ42 surface mean that the equilibrium amount of α-helix-containing Aβ42 conformers will be lower. The differential stability of α-helix-containing conformers of Aβ40 and Aβ42 explains the well-known difference between the two peptides in assembly rate—a difference that appears to be

related directly to the increased neurotoxicity of the longer Aβ alloform.[10]

Summary

The impetus for our work was the importance of elucidating alloform-specific differences in structural dynamics between Aβ40 and Aβ42—differences that appear to underlie the pathogenesis of AD. REMD simulations at microsecond timescale reproduced aspects of Aβ conformational dynamics that had been revealed previously using NMR, supporting the biological relevance of the simulations and, importantly, providing insights not obtainable experimentally. We find that neither peptide monomer is unstructured, but rather that each may be described as a unique statistical coil in which five relatively independent folding units exist, comprising residues 1–5, 10–13, 17–22, 28–37, and 39–42, which are connected by four turn structures. Incorporating this modular organization into folding algorithms could simplify analyses of Aβ assembly and facilitate *ab initio* studies of Aβ oligomerization. Our determination of the free-energy surfaces of Aβ40 and Aβ42 revealed that both peptides may possess significant amounts of α- or β-structure and that conformers within and between each structural class are in rapid equilibrium. The two additional hydrophobic residues at the Aβ42 C-terminus, Ile41 and Ala42, significantly increase contacts within the C-terminus and between the C-terminus and the CHC. As a result, the β-structure of Aβ42 is more stable than that of Aβ40, and the conformational equilibrium in Aβ42 shifts towards β-structure. Considered together with our previous studies of the role of α-helix formation in Aβ assembly,[71,72] these results suggest that drugs stabilizing α-helical Aβ conformers (or destabilizing the β-sheet state)[73] would block formation of neurotoxic oligomers. The atomic-resolution conformer structures determined in our simulations may serve as useful targets for this purpose.

Materials and Methods

Replica-exchange MD simulation

Our first consideration in selecting a method for simulating Aβ monomer conformational dynamics was how to model a highly flexible peptide chain that, in its extended conformation, is ~156 Å in length. A simulation space fully enclosing such a conformer would contain >100,000 water molecules. Simulations of systems of this size over meaningful timescales currently are computationally impractical. Solvating a more compact peptide conformer would produce a much smaller system. For example, a 50- to 60-Å simulation space would contain only ~5000 water molecules. However, natively disordered peptides sample extended states; when this occurs during a simulation, interimage interactions that would affect the results can occur. Even in situations in which a pronounced bias toward compact states exists, interconversion among different states likely would proceed through extended intermediates. For these reasons, we used the generalized Born (GB) implicit solvation model[74] to mimic the aqueous environment and did not represent water explicitly.

By eliminating the degrees of freedom and the viscosity associated with solvent water, simulations using the GB model can converge rapidly and explore conformational space efficiently. However, as with any simulation system, limitations exist. In the absence of explicit water, the simulated events take place much faster due to the lack of frictional effects. This complicates studies of kinetics. Our primary focus here is the thermodynamics of the systems, not their kinetics; thus, a more rapid attainment of equilibrium is useful. Another potential limitation of the GB model is that it does not allow the simulation of water bridges. However, for a highly flexible molecule such as Aβ, there is no evidence that water bridges contribute significantly to its stability. In practice, the GB approach has been implemented frequently and has yielded reliable results,[75–78] including results from *ab initio* protein folding experiments in which structures of unprecedented accuracy were produced.[79,80]

We used the REMD technique to further enhance conformational sampling. The simulations were performed with the Sander module of the Amber simulation package (version 9).[81] The proteins were modeled by PARM99SB, a recently improved Amber force field.[82] We implemented an effective 0.2 M salt concentration in the GB solvent model. Nonpolar solvation effects were represented using a surface tension coefficient of 0.005 kcal/mol Å^2. Starting from extended Aβ monomer, 16 replicas that exponentially spanned the temperature range 276–400 K were created. The temperature of the system was regulated using the Berendsen coupling algorithm[83] with a coupling constant of 1.0 ps. Hydrogen atoms were constrained using SHAKE.[84] The integration time step was 2 fs. Exchange between replicas was attempted every 2 ps. We used the default values of the Sander module for other relevant parameters.[81] This system mimics a very dilute aqueous Aβ solution at neutral pH. For each replica, the simulation length was 110 ns, and 110,000 conformations were collected. The first 10 ns was treated as equilibrium, and the last 100 ns was used for data analysis. The total simulation time was 3.52 μs.

Correlation of computationally and experimentally determined chemical shifts

Chemical shifts were determined from our simulation data using the SHIFTS program.[48] Correlation of these data with those obtained by NMR then was determined using the Pearson correlation coefficient (Eq. (1)):

$$r = \frac{\langle (x_i - \langle x \rangle)(y_i - \langle y \rangle) \rangle}{\sqrt{\langle (x_i - \langle x \rangle)^2 \rangle \langle (y_i - \langle y \rangle)^2 \rangle}} \quad (1)$$

Correlated motion

Isotropically distributed ensemble analysis[85] was used to characterize the correlated molecular motions of Aβ. We represent each residue with its corresponding C^α atom. For a protein containing n amino acids, we first constructed an $n \times n$ matrix $\mathbf{P}$ with elements $P_{ij} = \frac{1}{3}\langle \vec{r}_i \cdot \vec{r}_j \rangle$, where $\vec{r}_i$ (or $\vec{r}_i$), the position vector of residue i (or j), originates from the center of mass of the protein

and ends at each C^{α} atom. Each element P_{ij} of the matrix is the vector product averaged over the entire conformational ensemble. The cross-correlation coefficient $r_{ij} = P_{ij}/(P_i P_{jj})^{1/2}$, with the overall rotational modes eliminated. If $r_{i\,j} = 1$, the motions of the two residues i and j are highly positively correlated. If $r_{ij} = -1$, the motions are strongly negatively correlated. For $r_{ij} = 0$, no correlation exists.

Principal coordinate analysis

Energy surfaces were constructed by principal coordinate analysis.[70] To do so, the collected conformations were clustered with a threshold RMSD distance of 3.0 Å. The cluster centers were used to build a distance matrix **A** with elements $A_{ij} = -\frac{1}{2}d_{ij}^2$, where d_{ij} is the power distance[86] between conformations i and j. The matrix **A** was "centered" by Eq. (2), where $\langle \ldots \rangle_k$ is the mean over all specific indices $k = i, j, j$ or ij:

$$A_{ij}^{*} = A_{ij} - \langle A_{ij} \rangle_i - \langle A_{ij} \rangle_j + \langle A_{ij} \rangle_{ij} \quad (2)$$

This centering process guarantees a zero root of matrix **A***. Matrix **A*** was diagonalized, and the resulting eigenvectors were sorted in descending order according to their corresponding eigenvalues. Finally, we constructed the free-energy surface by projecting all the collected conformations onto the two-dimensional space defined by the first two eigenvectors. This procedure is similar to that described by Yang *et al.*, with the exception that the "minimum energy envelope" was not adopted.[75] The conformations in our analysis were not minimized, and *all* collected conformations were projected onto the surface to retain the free-energy information.

Acknowledgements

We gratefully acknowledge grants from the State of California Alzheimer's Disease Research Fund (no. 07-65806), the UCLA Faculty Research Grant program, the National Institutes of Health (AG027818), and the Jim Easton Consortium for Alzheimer's Drug Discovery and Biomarkers. Computational resources were provided by UCLA Academic Technology Services and the National Center for Supercomputing Applications. Use of the PyMOL and Gnuplot software packages (GPL-licensed) is gratefully acknowledged.

Supplementary Data

Supplementary data associated with this article can be found, in the online version, at doi:10.1016/j.jmb.2008.09.039

References

1. Plassman, B. L., Langa, K. M., Fisher, G. G., Heeringa, S. G., Weir, D. R., Ofstedal, M. B. *et al.* (2007). Prevalence of dementia in the United States: the aging, demographics, and memory study. *Neuroepidemiology*, **29**, 125–132.
2. Selkoe, D. J. (1991). The molecular pathology of Alzheimer's disease. *Neuron*, **6**, 487–498.
3. Hardy, J. A. & Higgins, G. A. (1992). Alzheimer's disease: the amyloid cascade hypothesis. *Science*, **256**, 184–185.
4. Kirkitadze, M. D., Bitan, G. & Teplow, D. B. (2002). Paradigm shifts in Alzheimer's disease and other neurodegenerative disorders: the emerging role of oligomeric assemblies. *J. Neurosci. Res.* **69**, 567–577.
5. Klein, W. L., Stine, W. B. & Teplow, D. B. (2004). Small assemblies of unmodified amyloid β-protein are the proximate neurotoxin in Alzheimer's disease. *Neurobiol. Aging*, **25**, 569–580.
6. Haass, C. & Selkoe, D. J. (2007). Soluble protein oligomers in neurodegeneration: lessons from the Alzheimer's amyloid β-peptide. *Nat. Rev. Mol. Cell Biol.* **8**, 101–112.
7. Necula, M., Breydo, L., Milton, S., Kayed, R., Veer, W., Tone, P. & Glabe, C. (2007). Methylene blue inhibits amyloid Aβ oligomerization by promoting fibrillization. *Biochemistry*, **46**, 8850–8860.
8. Necula, M., Kayed, R., Milton, S. & Glabe, C. G. (2007). Small molecule inhibitors of aggregation indicate that amyloid β oligomerization and fibrillization pathways are independent and distinct. *J. Biol. Chem.* **282**, 10311–10324.
9. Cheng, I. H., Scearce-Levie, K., Legleiter, J., Palop, J. J., Gerstein, H., Bien-Ly, N. *et al.* (2007). Accelerating amyloid-β fibrillization reduces oligomer levels and functional deficits in Alzheimer disease mouse models. *J. Biol. Chem.* **282**, 23818–23828.
10. Roychaudhuri, R., Yang, M. & Teplow, D. B. (2008) Amyloid β-protein assembly and Alzheimer's disease. *J. Biol. Chem.*, in press. doi:10.1074/jbc.R800036200.
11. Gravina, S. A., Ho, L., Eckman, C. B., Long, K. E., Otvos, L., Younkin, L. H. *et al.* (1995). Amyloid β protein (Aβ) in Alzheimer's disease brain. Biochemical and immunocytochemical analysis with antibodies specific for forms ending at Aβ 40 or Aβ42(43). *J. Biol. Chem.* **270**, 7013–7016.
12. Iwatsubo, T., Odaka, A., Suzuki, N., Mizusawa, H., Nukina, N. & Ihara, Y. (1994). Visualization of Aβ 42 (43) and Aβ 40 in senile plaques with end-specific Aβ monoclonals: Evidence that an initially deposited species is Aβ42(43). *Neuron*, **13**, 45–53.
13. Suzuki, N., Cheung, T. T., Cai, X. D., Odaka, A., Otvos, L., Eckman, C. *et al.* (1994). An increased percentage of long amyloid β-protein secreted by familial amyloid β-protein precursor (β APP717) mutants. *Science*, **264**, 1336–1340.
14. Golde, T. E., Eckman, C. B. & Younkin, S. G. (2000). Biochemical detection of Aβ isoforms: implications for pathogenesis, diagnosis, and treatment of Alzheimer's disease. *Biochim. Biophys. Acta*, **1502**, 172–187.
15. Scheuner, D., Eckman, C., Jensen, M., Song, X., Citron, M., Suzuki, N. *et al.* (1996). Secreted amyloid β-protein similar to that in the senile plaques of Alzheimer's disease is increased *in vivo* by the presenilin 1 and 2 and APP mutations linked to familial Alzheimer's disease. *Nat. Med.* **2**, 864–870.
16. Weggen, S., Eriksen, J. L., Das, P., Sagi, S. A., Wang, R., Pietrzik, C. U. *et al.* (2001). A subset of NSAIDs lower amyloidogenic Aβ42 independently of cyclooxygenase activity. *Nature*, **414**, 212–216.
17. Dahlgren, K. N., Manelli, A. M., Stine, W. B., Baker, L. K., Krafft, G. A. & LaDu, M. J. (2002). Oligomeric and fibrillar species of amyloid-β peptides differentially affect neuronal viability. *J. Biol. Chem.* **277**, 32046–32053.

18. Selkoe, D. J. (1999). Translating cell biology into therapeutic advances in Alzheimer's disease. *Nature*, **399**, A23–A31.
19. Younkin, S. G. (1995). Evidence that Aβ42 is the real culprit in Alzheimer's disease. *Ann. Neurol.* **37**, 287–288.
20. Jarrett, J. T., Berger, E. P. & Lansbury, P. T. (1993). The carboxy terminus of the β amyloid protein is critical for the seeding of amyloid formation: implications for the pathogenesis of Alzheimer's disease. *Biochemistry*, **32**, 4693–4697.
21. Lomakin, A., Chung, D. S., Benedek, G. B., Kirschner, D. A. & Teplow, D. B. (1996). On the nucleation and growth of amyloid β-protein fibrils: detection of nuclei and quantitation of rate constants. *Proc. Natl Acad. Sci. USA*, **93**, 1125–1129.
22. Lomakin, A., Teplow, D. B., Kirschner, D. A. & Benedek, G. B. (1997). Kinetic theory of fibrillogenesis of amyloid β-protein. *Proc. Natl Acad. Sci. USA*, **93**, 7942–7947.
23. Chen, Y.-R. & Glabe, C. G. (2006). Distinct early folding and aggregation properties of Alzheimer amyloid-β peptides Aβ 40 and Aβ 42: Stable trimer or tetramer formation by Aβ42. *J. Biol. Chem.* **94**, 24414–24422.
24. Bitan, G., Kirkitadze, M. D., Lomakin, A., Vollers, S. S., Benedek, G. B. & Teplow, D. B. (2003). Amyloid β-protein (Aβ) assembly: Aβ40 and Aβ42 oligomerize through distinct pathways. *Proc. Natl Acad. Sci. USA*, **100**, 330–335.
25. Teplow, D. B. (2006). Preparation of amyloid β-protein for structural and functional studies. *Methods Enzymol.* **413**, 20–33.
26. Petkova, A. T., Leapman, R. D., Guo, Z., Yau, W.-M., Mattson, M. P. & Tycko, R. (2005). Self-propagating, molecular-level polymorphism in Alzheimer's β-amyloid fibrils. *Science*, **307**, 262–265.
27. Lee, J. P., Stimson, E. R., Ghilardi, J. R., Mantyh, P. W., Lu, Y. A., Felix, A. M. *et al.* (1995). ^{1}H NMR of Aβ amyloid peptide congeners in water solution. Conformational changes correlate with plaque competence. *Biochemistry*, **34**, 5191–5200.
28. Jarvet, J., Damberg, P., Bodell, K., Eriksson, L. E. G. & Graslund, A. (2000). Reversible random coil to β-sheet transition and the early stage of aggregation of the Aβ(12–28) fragment from the Alzheimer peptide. *J. Am. Chem. Soc.* **122**, 4261–4268.
29. Lazo, N. D., Grant, M. A., Condron, M. C., Rigby, A. C. & Teplow, D. B. (2005). On the nucleation of amyloid β-protein monomer folding. *Protein Sci.* **14**, 1581–1596.
30. Takano, K., Endo, S., Mukaiyama, A., Chon, H., Matsumura, H., Koga, Y. & Kanaya, S. (2006). Structure of amyloid β fragments in aqueous environments. *FEBS J.* **273**, 150–158.
31. Zhang, S., Iwata, K., Lachenmann, M. J., Peng, J. W., Li, S., Stimson, E. R. *et al.* (2000). The Alzheimer's peptide Aβ adopts a collapsed coil structure in water. *J. Struct. Biol.* **130**, 130–141.
32. Hou, L., Shao, H., Zhang, Y., Li, H., Menon, N. K., Neuhaus, E. B. *et al.* (2004). Solution NMR studies of the Aβ(1–40) and Aβ(1–42) peptides establish that the Met35 oxidation state affects the mechanism of amyloid formation. *J. Am. Chem. Soc.* **126**, 1992–2005.
33. Lim, K. H., Collver, H. H., Le, Y. T. H., Nagchowdhuri, P. & Kenney, J. M. (2007). Characterizations of distinct amyloidogenic conformations of the Aβ (1–40) and (1–42) peptides. *Biochem. Biophys. Res. Commun.* **364**, 443–449.
34. Yan, Y. & Wang, C. (2006). Aβ42 is more rigid than Aβ40 at the C terminus: Implications for Aβ aggregation and toxicity. *J. Mol. Biol.* **364**, 853–862.
35. Riek, R., Gntert, P., Dbeli, H., Wipf, B. & Wthrich, K. (2001). NMR studies in aqueous solution fail to identify significant conformational differences between the monomeric forms of two Alzheimer peptides with widely different plaque-competence, Aβ(1–40)(ox) and Aβ1–42)(ox). *Eur. J. Biochem.* **268**, 5930–5936.
36. Barrow, C. J. & Zagorski, M. G. (1991). Solution structures of β peptide and its constituent fragments: relation to amyloid deposition. *Science*, **253**, 179–182.
37. Barrow, C. J., Yasuda, A., Kenny, P. T. & Zagorski, M. G. (1992). Solution conformations and aggregational properties of synthetic amyloid β-peptides of Alzheimer's disease. Analysis of circular dichroism spectra. *J. Mol. Biol.* **225**, 1075–1093.
38. Crescenzi, O., Tomaselli, S., Guerrini, R., Salvadori, S., DUrsi, A. M., Temussi, P. A. & Picone, D. (2002). Solution structure of the Alzheimer amyloid β-peptide (1–42) in an apolar microenvironment. Similarity with a virus fusion domain. *Eur. J. Biochem.* **269**, 5642–5648.
39. Sticht, H., Bayer, P., Willbold, D., Dames, S., Hilbich, C., Beyreuther, K. *et al.* (1995). Structure of amyloid A4-(1–40)-peptide of Alzheimer's disease. *Eur. J. Biochem.* **233**, 293–298.
40. Tomaselli, S., Esposito, V., Vangone, P., van Nuland, N. A. J., Bonvin, A. M. J. J., Guerrini, R. *et al.* (2006). The α-to-β conformational transition of Alzheimer's Aβ-(1–42) peptide in aqueous media is reversible: A step by step conformational analysis suggests the location of β conformation seeding. *ChemBioChem*, **7**, 257–267.
41. Coles, M., Bicknell, W., Watson, A. A., Fairlie, D. P. & Craik, D. J. (1998). Solution structure of amyloid β-peptide(1–40) in a water–micelle environment. Is the membrane-spanning domain where we think it is? *Biochemistry*, **37**, 11064–11077.
42. Shao, H., Jao, S., Ma, K. & Zagorski, M. G. (1999). Solution structures of micelle-bound amyloid β-(1–40) and β-(1–42) peptides of Alzheimer's disease. *J. Mol. Biol.* **285**, 755–773.
43. Ma, B. & Nussinov, R. (2006). Simulations as analytical tools to understand protein aggregation and predict amyloid conformation. *Curr. Opin. Chem. Biol.* **10**, 445–452.
44. Teplow, D. B., Lazo, N. D., Bitan, G., Bernstein, S., Wyttenbach, T., Bowers, M. T. *et al.* (2006). Elucidating amyloid β-protein folding and assembly: A multidisciplinary approach. *Acc. Chem. Res.* **39**, 635–645.
45. Urbanc, B., Cruz, L., Teplow, D. B. & Stanley, H. E. (2006). Computer simulations of Alzheimer's amyloid β-protein folding and assembly. *Curr. Alzheimer Res.* **3**, 493–504.
46. Baumketner, A., Bernstein, S. L., Wyttenbach, T., Bitan, G., Teplow, D. B., Bowers, M. T. & Shea, J.-E. (2006). Amyloid β-protein monomer structure: a computational and experimental study. *Protein Sci.* **15**, 420–428.
47. Sgourakis, N. G., Yan, Y., McCallum, S. A., Wang, C. & Garcia, A. E. (2007). The Alzheimer's peptides Aβ40 and 42 adopt distinct conformations in water: A combined MD/NMR study. *J. Mol. Biol.* **368**, 1448–1457.
48. Xu, X. P. & Case, D. A. (2001). Automated prediction of ^{15}N, $^{13}C_{\alpha}$, $^{13}C_{\alpha}$ and $^{13}C'$ chemical shifts in proteins using a density functional database. *J. Biomol. NMR*, **21**, 321–333.

49. Xu, X.-P. & Case, D. A. (2002). Probing multiple effects on ^{15}N, $^{13}C_\alpha$, $^{13}C_\alpha$ and $^{13}C'$ chemical shifts in peptides using density functional theory. *Biopolymers*, **65**, 408–423.
50. Frishman, D. & Argos, P. (1995). Knowledge-based protein secondary structure assignment. *Proteins*, **23**, 566–579.
51. Kabsch, W. & Sander, C. (1983). Dictionary of protein secondary structure: pattern recognition of hydrogen-bonded and geometrical features. *Biopolymers*, **22**, 2577–2637.
52. Lansbury, P. (1999). Evolution of amyloid: What normal protein folding may tell us about fibrillogenesis and disease. *Proc. Natl Acad. Sci. USA*, **96**, 3342–3344.
53. Grant, M. A., Lazo, N. D., Lomakin, A., Condron, M. M., Arai, H., Yamin, G. *et al.* (2007). Familial Alzheimer's disease mutations alter the stability of the amyloid β-protein monomer folding nucleus. *Proc. Natl Acad. Sci. USA*, **104**, 16522–16527.
54. Borreguero, J. M., Urbanc, B., Lazo, N. D., Buldyrev, S. V., Teplow, D. B. & Stanley, H. E. (2005). Folding events in the 21–30 region of amyloid β-protein (Aβ) studied *in silico*. *Proc. Natl Acad. Sci. USA*, **102**, 6015–6020.
55. Baumketner, A., Bernstein, S. L., Wyttenbach, T., Lazo, N. D., Teplow, D. B., Bowers, M. T. & Shea, J. -E. (2006). Structure of the 21–30 fragment of amyloid β-protein. *Protein Sci.* **15**, 1239–1247.
56. Chen, W., Mousseau, N. & Derreumaux, P. (2006). The conformations of the amyloid-β (21–30) fragment can be described by three families in solution. *J. Chem. Phys.* **125**, 084911.
57. Fawzi, N. L., Phillips, A., Ruscio, J., Doucleff, M., Wemmer, D. & Head-Gordon, T. (2008). Structure and dynamics of the Aβ21–30 peptide from the interplay of NMR experiments and molecular simulations. *J. Am. Chem. Soc.* **130**, 6145–6158.
58. Tarus, B., Straub, J. E. & Thirumalai, D. (2006). Dynamics of Asp23-Lys28 salt-bridge formation in $A\beta_{10-35}$ monomers. *J. Am. Chem. Soc.* **128**, 16159–16168.
59. Urbanc, B., Cruz, L., Yun, S., Buldyrev, S. V., Bitan, G., Teplow, D. B. & Stanley, H. E. (2004). *In silico* study of amyloid β-protein folding and oligomerization. *Proc. Natl Acad. Sci. USA*, **101**, 17345–17350.
60. Maji, S. K., Amsden, J. J., Rothschild, K. J., Condron, M. M. & Teplow, D. B. (2005). Conformational dynamics of amyloid β-protein assembly probed using intrinsic fluorescence. *Biochemistry*, **44**, 13365–13376.
61. Maji, S. K., Loo, R. R. O., Spring, S. M., Vollers, S. S., Condron, M. M., Bitan, G. *et al.* (2008) Amino acid position-specific contributions to amyloid β-protein oligomerization. *J. Biol. Chem.*, submitted.
62. Fitzkee, N. C. & Rose, G. D. (2004). Reassessing random-coil statistics in unfolded proteins. *Proc. Natl Acad. Sci. USA*, **101**, 12497–12502.
63. Tran, H., Wang, X. & Pappu, R. (2005). Reconciling observations of sequence-specific conformational propensities with the generic polymeric behavior of denatured proteins. *Biochemistry*, **44**, 11369–11380.
64. Ichiye, T. & Karplus, M. (1991). Collective motions in proteins: a covariance analysis of atomic fluctuations in molecular dynamics and normal mode simulations. *Proteins*, **11**, 205–217.
65. Lührs, T., Ritter, C., Adrian, M., Riek-Loher, D., Bohrmann, B., Beli, H. D. *et al.* (2005). 3D structure of Alzheimer's amyloid-β(1–42) fibrils. *Proc. Natl Acad. Sci. USA*, **102**, 17342–17347.
66. Petkova, A. T., Yau, W. -M. & Tycko, R. (2006). Experimental constraints on quaternary structure in Alzheimer's β-amyloid fibrils. *Biochemistry*, **45**, 498–512.
67. Kusumoto, Y., Lomakin, A., Teplow, D. B. & Benedek, G. B. (1998). Temperature dependence of amyloid β-protein fibrillization. *Proc. Natl Acad. Sci. USA*, **95**, 12277–12282.
68. Esler, W. P., Felix, A. M., Stimson, E. R., Lachenmann, M. J., Ghilardi, J. R., Lu, Y. A. *et al.* (2000). Activation barriers to structural transition determine deposition rates of Alzheimer's disease Aβ amyloid. *J. Struct. Biol.* **130**, 174–183.
69. Massi, F. & Straub, J. E. (2001). Energy landscape theory for Alzheimer's amyloid β-peptide fibril elongation. *Proteins: Struct. Funct. Genet.* **42**, 217–229.
70. Becker, O. M. (1998). Principal coordinate maps of molecular potential energy surfaces. *J. Comput. Chem.* **19**, 1255–1267.
71. Kirkitadze, M. D., Condron, M. M. & Teplow, D. B. (2001). Identification and characterization of key kinetic intermediates in amyloid β-protein fibrillogenesis. *J. Mol. Biol.* **312**, 1103–1119.
72. Fezoui, Y. & Teplow, D. B. (2002). Kinetic studies of amyloid β-protein fibril assembly. Differential effects of α-helix stabilization. *J. Biol. Chem.* **277**, 36948–36954.
73. Rauk, A. (2008). Why is the amyloid beta peptide of Alzheimer's disease neurotoxic? *Dalton Trans.* **10**, 1273–1282.
74. Mongan, J., Simmerling, C., McCammon, J. A., Case, D. A. & Onufriev, A. (2006). Generalized Born model with a simple, robust molecular volume correction. *J. Chem. Theory Comput.* **3**, 156–159.
75. Yang, M., Yordanov, B., Levy, Y., Brüschweiler, R. & Huo, S. (2006). The sequence-dependent unfolding pathway plays a critical role in the amyloidogenicity of transthyretin. *Biochemistry*, **45**, 11992–12002.
76. Mongan, J., Case, D. A. & McCammon, J. A. (2004). Constant pH molecular dynamics in generalized Born implicit solvent. *J. Comput. Chem.* **25**, 2038–2048.
77. Morozov, A. V., Havranek, J. J., Baker, D. & Siggia, E. D. (2005). Protein–DNA binding specificity predictions with structural models. *Nucleic Acids Res.* **33**, 5781–5798.
78. Ashworth, J., Havranek, J. J., Duarte, C. M., Sussman, D., Monnat, R. J., Stoddard, B. L. & Baker, D. (2006). Computational redesign of endonuclease DNA binding and cleavage specificity. *Nature*, **441**, 656–659.
79. Lei, H., Wu, C., Liu, H. & Duan, Y. (2007). Folding free-energy landscape of villin headpiece subdomain from molecular dynamics simulations. *Proc. Natl Acad. Sci. USA*, **104**, 4925–4930.
80. Lei, H. & Duan, Y. (2007). Two-stage folding of HP-35 from *ab initio* simulations. *J. Mol. Biol.* **370**, 196–206.
81. Case, D. A., Cheatham, T. E., Darden, T., Gohlke, H., Luo, R., Merz, K. M. *et al.* (2005). The Amber biomolecular simulation programs. *J. Comput. Chem.* **26**, 1668–1688.
82. Hornak, V., Abel, R., Okur, A., Strockbine, B., Roitberg, A. & Simmerling, C. (2006). Comparison of multiple Amber force fields and development of improved protein backbone parameters. *Proteins*, **65**, 712–725.
83. Berendsen, H. J. C., Postma, J. P. M., van Gunsteren, W. F., DiNola, A. & Haak, J. R. (1984). Molecular dynamics with coupling to an external bath. *J. Chem. Phys.* **81**, 3684–3690.

84. Ryckaert, J.-P., Ciccotti, G. & Berendsen, H. J. C. (1977). Numerical integration of the Cartesian equations of motion of a system with constraints: molecular dynamics of *n*-alkanes. *J. Comput. Phys.* **23**, 327–341.
85. Prompers, J. J. & Brüschweiler, R. (2002). Dynamic and structural analysis of isotropically distributed molecular ensembles. *Proteins*, **46**, 177–189.
86. Wallin, S., Farwer, J. & Bastolla, U. (2003). Testing similarity measures with continuous and discrete protein models. *Proteins*, **50**, 144–157.